Received: 6 April 2024 | Revised: 30 April 2024 | Accepted: 17 May 2024

IET Quantum Communication

DOI: 10.1049/qtc2.12097

The Institution of Engineering and Technology WILEY

ORIGINAL RESEARCH

Experimental feasibility analysis of quantum/classical coexistence over fibre and free space links

Aristeidis Stathis | **Argiris Ntanos** | **Panagiotis Toumasis** | **Nikolaos K. Lyras** | **Giannis Giannoulis** | **Hercules Avramopoulos**

School of Electrical and Computer Engineering, National Technical University of Athens, Zografou, Athens, Greece

Correspondence

Aristeidis Stathis.
Email: stathisaris@mail.ntua.gr

Funding information

Quantum Secure Network Partnership, Grant/Award Number: 101114043

Abstract

The authors present a novel approach to Quantum Key Distribution (QKD) research, emphasising cost-effectiveness and practicality using a single photon polarisation-encoded system employing mainly commercial off-the-shelf components. This study diverges from previous high-cost, high-end setups by exploring the viability of QKD in more accessible and realistic settings. Our approach focuses on practical measurements of the signal-to-noise ratio by analysing polarisation-encoded photonic qubits over various transmission scenarios. The authors introduce a simplified evaluation method that incorporates experimental measurements, such as noise sources and losses, into a semi-empirical theoretical framework. This framework simulates the standard DS-BB84 protocol to estimate Secure Key Rates (SKRs), offering an alternative approach on the evaluation of the practical implementation of QKD. Specifically, the authors examine the feasibility of QKD over a 2.2 km intra-campus fibre link in coexistence scenarios, identifying optimal Wavelength-Division Multiplexing allocations to minimise Raman noise, achieving an expected SKR of up to 300 bps. Additionally, the authors' study extends to 40 m indoor and 100 m outdoor Free-Space Optical (FSO) links using low-cost components, where the authors recorded Quantum Bit Error Rate (QBER) values below 3.2%, allowing for possible SKRs up to 600 bps even in daylight operation. The converged fibre/FSO scenario demonstrated robust performance, with QBER values below 3.7% and an expected SKR of over 200 bps. Our research bridges the gap between high-end and economical QKD solutions, providing valuable insights into the feasibility of QKD in everyday scenarios, especially within metropolitan fibre based and FSO links. By leveraging cost-effective components and a simplified single photon exchange setup, the authors work paves the way for the effortless characterisation of deployed infrastructure, highlighting its potential in diverse settings and its accessibility for widespread implementation.

KEYWORDS

optical fibre networks, quantum communication, quantum cryptography

1 | INTRODUCTION

Quantum Key Distribution (QKD) represents a promising solution for ensuring secure communication by leveraging the fundamental principles of quantum mechanics to exchange cryptographic keys, offering unparalleled security [1]. In contrast to the widespread use of optical fibres for integrating QKD systems into existing network infrastructure, valued for their low-loss transmission and remarkable stability, Free-Space Optical (FSO) links have gained significant interest as a readily deployable solution. The first demonstration of terrestrial FSO-QKD showed up in the early 2000s. One of the earliest

milestones was set by the Los Alamos National Laboratory in 2002, where researchers implemented a polarisation-encoded BB84 protocol over a 10 km FSO link, demonstrating its feasibility during both daylight and night conditions [2]. Subsequently, in 2005, a significant experiment was conducted at Dashu Mountain in Hefei, China, where the free-space distribution of entangled photon pairs, at a wavelength of 702 nm, was achieved over a noisy ground atmosphere of 13 km at night [3]. This was followed by the groundbreaking experiment in the Canary Islands in 2007, involving the EU, UK, and European Space Agency [4]. This experiment successfully executed polarisation-encoded DS-BB84 and ENT-based QKD over a 144 km distance between the islands of La Palma and Tenerife, predominantly during night hours. Regarding fibre-based QKD, the significant cost escalation associated with the allocation of dedicated fibres solely for QKD purposes underscores the prominence of Raman noise, which poses the primary obstacle in scenarios involving the coexistence of quantum and classical signals over the same fibre core. Towards this direction, noise filtering techniques have enabled a deployment-friendly approach [5]. In contrast, FSO links offer a transmission where non-linear effects such as Spontaneous Raman Scattering (SpRS) are no longer present; however, they remain vulnerable to environmental conditions and solar noise radiance, whereas ensuring precise pointing stability can become challenging. To address these challenges, particularly in long-distance FSO links, mitigation techniques such as Fast Steering Mirrors and Adaptive Optics (AO) are employed to compensate for these losses [6]. Shifting the emphasis to metropolitan networks, the convergence of fibre and free-space access domains is anticipated. In this configuration, quantum links seamlessly coexist with intense classical optical signals within established fibre topologies, extending their reach by propagating wirelessly in free-space point-to-point links. In 2021, the University of Padua in Italy enabled full daylight QKD using 1550 nm silicon photonics over a 145m FSO link in an urban transmission scenario [7]. Recent noteworthy achievements include the successful demonstration of an FSO/fibre QKD link in Shanghai's urban setting [8], where researchers demonstrated a FSO-QKD experiment using polarisation-encoded photons at 1550 nm, over a 53 km link in daylight conditions. Similarly, experimental campaigns in Vienna and Padova have showcased sub-kilometre FSO links alongside dark fibre installations tailored for QKD transmission [9]. In 2023, significant advancements were observed across various European locations regarding FSO-QKD. In Jena, Germany, a deployable free-space QKD link utilising an 810 nm Entangled Photon Source was established, effectively bridging a 1.7-km noisy metropolitan link. This innovation marks a leap in secure communication technology. Simultaneously, collaborative efforts between Padova, Italy, and Vienna, Austria, led to groundbreaking intermodal-QKD field trials. These trials successfully integrated fibre networks with free-space channels to operate polarisation-encoded QKD links at 1550 nm, showcasing resilience under varying conditions including daylight and rain [10]. Further enhancing the robustness of QKD, the Institute for Quantum Optics and Quantum Information in Vienna conducted a high-dimensional QKD experiment over a noisy 10.2 km metropolitan free-space channel [11]. This experiment demonstrated a significant advantage in noise resistance, heralding a new era of secure communication over longer and environmentally challenging distances.

While these significant research milestones underscore the groundbreaking advancements in QKD, particularly in the context of integrating these systems into existing network infrastructures using both fibres and FSO links, our work contributes to this evolving field from a different perspective. Our goal is not to demonstrate a full-scale polarisation-encoded QKD setup but to propose an easily installed experiment providing a reliable feasibility analysis for future QKD deployments in the links under test. Unlike the large-scale deployments which often involve state-of-the-art costly setups, our study explores the viability of QKD using more accessible and cost-effective deployment. By utilising a simplified setup comprised mainly of commercial off-the-shelf polarisation optics and a pair of Single Photon Detectors (SPDs) [12], we facilitate practical measurements of signal-to-noise ratio (i.e. Quantum Bit Error Rate (QBER) by analysing a prepared photonic qubit over an orthogonal polarisation basis in various transmission scenarios. Our approach simplifies the evaluation of various link setups without the need for complicated post processing units. To complement our experimental setup, we developed a semi-empirical theoretical toolbox which can be fed with experimental measurements such as the overall noise, the link's transmittance along with the system assumptions (e.g. SPDs detection parameters), to calculate the expected signal gain by simulating the standard DS-BB84 protocol, thus allowing the estimation of the expected Secure Key Rates (SKRs). To evaluate our proposed scheme various transmission topologies including fibre/FSO and converged fibre/FSO scenarios have been investigated both with and without classical signal transmission coexisting along with the quantum signal. Specifically, to study the optimised classical/quantum coexistence, the most effective Wavelength-Division Multiplexing (WDM) allocation was explored for minimising the Raman noise in a fibre-based coexistence scenario revealing an expected SKR of up to 300 bps for the best WDM allocation. Regarding the free space segment, a 40-m indoor and a 100-m outdoor FSO link are established with low-cost components, evaluating their performance under conditions where quantum and classical signals coexist. Quantum Bit Error Rate values below 3.2% were recorded, suggesting a possible SKR of up to 600 bps for operations conducted during both day and night, while the converged fibre/FSO scenario demonstrated robust performance under coexistence scenarios, showing QBER values below 3.7% and 3.9%, respectively, with an expected SKRs of more than 200 bps. The reported methodology provides a valuable experimental tool for the researchers and scientists working on the design phase for assessing QKD technologies. The simplicity of the setup, which includes readily available components, enables practical measurements

of signal-to-noise ratio and allows for straightforward link characterisation and performance estimation in terms of SKR. The remainder of the paper is structured as follows: Section 2 provides a detailed presentation of the experimental reference setup for multiplexing classical and quantum signals in the deployed infrastructure, while Section 3 discusses the different transmission scenarios. The obtained experimental results are presented in section 4, where the proposed classical/quantum coexistence setup is also evaluated through the simulation toolbox. Finally, section 5 summarises and concludes the manuscript.

2 | EXPERIMENTAL SETUP AND METHODOLOGY

2.1 | Experimental setup

Figure 1 depicts the experimental layout which is based on weak coherent light, COTS-based polarisation optics and a pair of InGaAs Single Photon Avalanche Diodes (SPADs). In what follows, a detailed breakdown of the experimental setup will be presented.

2.1.1 | Sender station

On the sender station's side, quantum pulses are produced utilising a Continuous Wavelength (CW) laser source emitting at 1550.12 nm. The laser is modulated at a repetition rate of 10 MHz via a Ti:LiNbO3 Mach–Zehnder Modulator (MZM¬) (FTM7921ER) driven by an Arbitrary Waveform Generator (AWG) (Keysight 33600A 80 MHz Trueform Waveform Generator). Optical power levels are carefully adjusted to achieve the desired mean photon numbers through cascaded attenuation stages. To determine the mean photon number, we directly measured the count rate at the receiver. From this number (at a given repetition rate), μ can be extracted by using the receiver transmission, the specified efficiency of the detectors ($\eta = 10\%$) and accounting for the deadtime correction of the detectors at high count rates. For the evaluation of the performance across the different transmission scenarios, solely the vertical polarisation encoding is prepared, with the use of a Polarisation Beam Splitter (PBS) in the emission stage. An Optical Power Monitor is used after the PBS to monitor any polarisation drifts, thus maintaining the intensity of the quantum channel stable.

2.1.2 | Receiver station

In the detection setup, a two-stage Band-Pass Filter, featuring cascaded passbands of 0.1-nm (Finisar DWP-EK-AA, IL = 4.5 dB, Suppression Ratio (SR) = 40 dB) and 0.2-nm (OPNETI C34 ITU-grid 25 GHz dense wavelength division multiplexing (DWDM), IL = 1.5 dB, SR = 30 dB), respectively, with a total loss of 6 dB, was used to isolate the quantum signal. The polarisation state at the receiver's end was adjusted to align with the transmission axis of the PBS using a Motorised Polarisation Controller (Thorlabs, MPC). As a result, the quantum signal was exclusively directed to one of the two InGaAs SPADs, enabling the conductance of photon counting and QBER measurements. The SPAD units (AUREA OEM_NIR) operated with $\eta = 10\%$ quantum efficiency (Q.E) in a gated mode (6 ns gate) and a 20-µs dead time, thus constraining the SPADs' afterpulsing probability to approximately 2%.

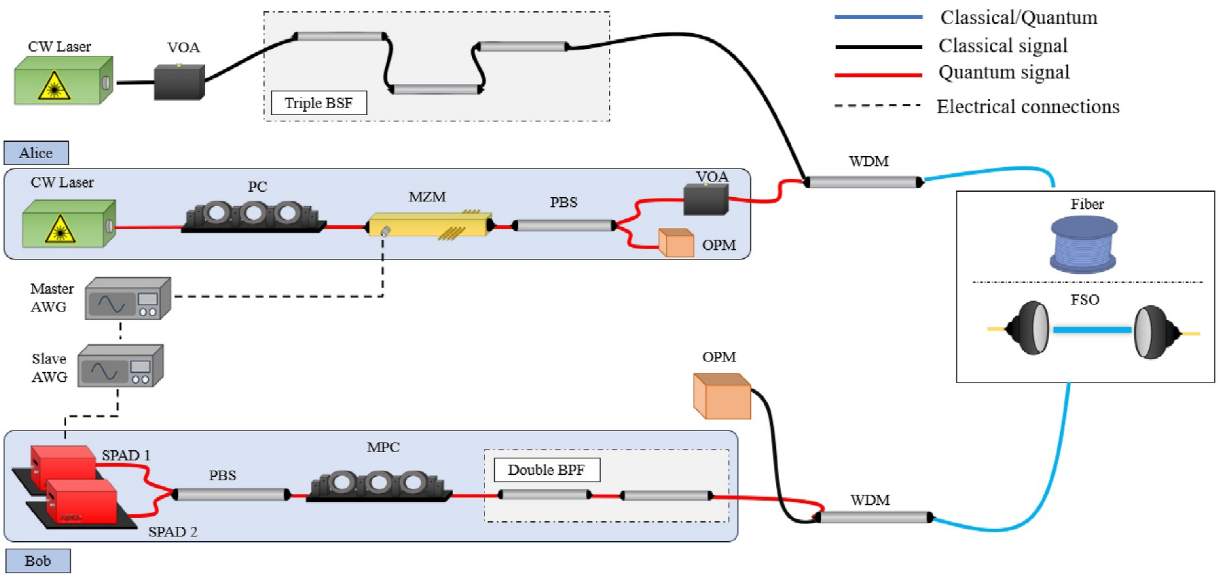

FIGURE 1 Single photon polarisation-encoded layout for classical/quantum coexistence over fibre or free space links. ***Sender Station***: Coherent laser source is carved into pulses with a MZM and attenuated to sub-photon levels per pulse using a VOA. ***Receiver Station***: Consists of two cascaded BPF, an MPC, a PBS and the two SPADs. BPF, Band-Pass Filter; PBS, Polarization Beam Splitter; SPADs, Single Photon Avalanche Diodes; VOA, variable optical attenuator.

2.1.3 | Coexistence zone

For the coexistence scenarios presented in this work, a tunable CW laser is used to choose the classical wavelength/s that will eventually coexist with the quantum pulses. The quantum signal is multiplexed with one or multiple CW lasers using a 16-channel 100 GHz DWDM module for C-Band (Texas Instruments) with various launch power intensities controlled by a variable optical attenuator. To minimise noise photon interference within the quantum passband in the coexistence scenarios, a triple-stage notch filter (C34 ITU-grid DWDM 100 GHz modules) with a narrow stopband of 0.8 nm, a total Insertion Loss (IL)of 1.5 dB and a SR of 175 dB, respectively, was also added to the classical signal prior to its transmission.

2.1.4 | Synch

For the synchronisation, two AWGs (Keysight 33600A 80 MHz Trueform Waveform Generator) were electrically locked using the 10 MHz Transistor–Transistor Logic internal reference clock provided by the master AWG. The master AWG was used to drive the MZM, whereas the second AWG (slave) applied the gating voltage input in the SPADs. To facilitate the experiment, the two AWGs were in the same room. It is also worth noting that the remote locking of the AWGs is also possible by feeding the external reference clock of the AWG in a MZM to convert the electrical signal into optical and distribute it through optical fibres. In the receiving end, the clock will be recovered using a photoreceiver (InGaAs Optical Receiver, Discovery Semiconductors) and will be fed to the external input of the slave AWG, enabling the synchronisation of the two AWGs.

2.2 | Transmission scenarios

Table 1 presents a summary of the different transmission configuration scenarios that have been investigated and will be presented in the following sections. Figure 2 shows the infrastructure in which the classical/quantum feasibility campaigns took place. For the fibre segment, a 2.2-km Intra-Campus (IC) fibre link installed within the premises of the National Technical University of Athens (NTUA) was utilised, interconnecting the Photonics Communication Research Laboratory (PCRL) with NTUA's Network Operation Centre (Figure 2a). As for the free-space segment, two testbeds were employed. The first FSO testbed was set up indoors at the PCRL, covering approximately 40 m (Figure 2b), while the second was established outdoors on the rooftops of the School of Electrical and Computer Engineering, bridging different buildings over a distance exceeding 100 m (Figure 2c). The scenarios tested also included converged topologies, that is, fibre transmission followed by FSO transmission. For each transmission scenario, a characterisation campaign was conducted to determine/estimate link parameters such as the Raman noise in the fibres as well as to calculate the link budget for the case of the FSO links as a function of distance.

TABLE 1 Transmission scenarios.

#	Fibre	Free space	CW channels
S1	-	40 m Indoor	1 SFP
S2	2.2 km IC	40 m Indoor	1 SFP
S3	2.2 km IC	-	4 CW
S4	-	40 m Indoor	4 CW
S5	-	100 m Outdoor (night)	1 CW
S6	-	100 m Outdoor (day)	1 CW

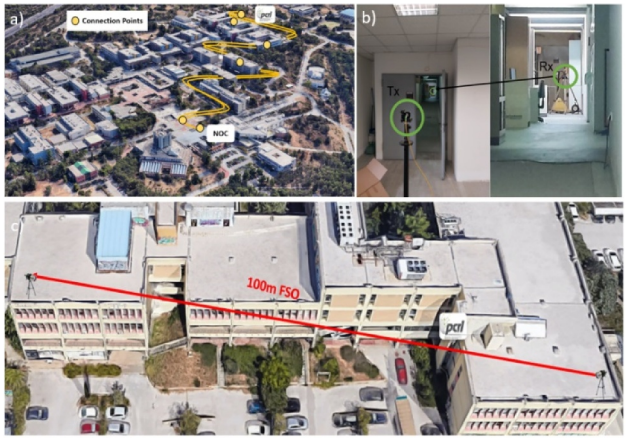

FIGURE 2 (a) Installed intra-campus 2.2-km fibre link, (b) 40-m indoor FSO link, (c) Map of 100-m FSO link interconnecting two ECE building's rooftops [©2024 Google]. ECE, Electrical and Computer Engineering; FSO, Free-Space Optical; IC, Intra-Campus.

2.2.1 | Fibre segment

More specifically, Optical Domain Reflectometry studies were conducted to evaluate the losses of the IC fibre. The optical losses introduced by the 2.2-km fibre were determined to be 4.5 dB due to the multiple connection points (~18). After characterising the losses of the fibre, we experimentally measured the Raman noise profile in both backward and forward propagation direction. This step was taken to determine the optimal wavelength allocation for the coexistence measurements in the subsequent phase of the experiment. To determine the Raman noise leaking into the quantum passband, we scanned the wavelength of a tunable CW laser to determine the volume of the SpRS noise generated from a single optical classical channel within the telecom C-band as reported in detail elsewhere [13]. Figure 3 below presents the Raman noise counts in the quantum passband (1550.12 nm) for different allocations of the classical wavelength propagating in both backward and forward direction, normalised with respect to noise generated at 1551.79 nm for the 2.2-km IC fibre.

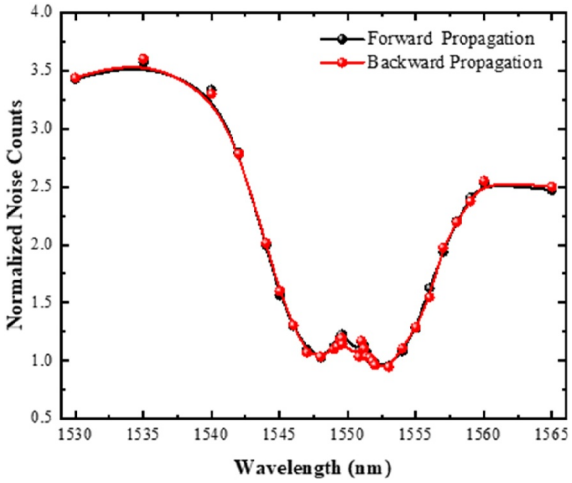

FIGURE 3 Forward and Backward Raman noise photons for the 2.2-km IC fibre. IC, Intra-Campus.

The Raman noise profile is in good agreement with what has been reported in the literature for standard SMFs [5]. For this wavelength, the noise was measured in a free-running mode to be 17.5 and 3.7 kcps for 2.2-km transmission, respectively, for both forward and backward direction. The Raman measurement campaign allowed us to calculate the Raman cross-section coefficient $\varrho(\lambda)$ for each fibre using Equations (3) and (4) below [5]:

$$P_{ram},f = P_{in} \times e^{-a \cdot L} \times L \times \rho(\lambda) \times \Delta\lambda, \quad (1)$$

$$P_{ram},b = P_{in} \times e^{-a \cdot L} \times \frac{\sinh{(a \cdot L)}}{a} \times \rho(\lambda) \times \Delta\lambda, \quad (2)$$

here, P_{in} is the power at the fibre input (W), α is the fibre attenuation coefficient (km^{-1}), $\varrho(\lambda)$ is the wavelength dependent Raman cross-section coefficient, L is the fibre length (km) and $\Delta\lambda$ accounts for the optical filter passband in the receiver station. By experimentally measuring the P_{ram}, f, P_{ram}, b and by knowing the launched power P_{in}, we solved Equations (1) and (2) with respect to $\rho(\lambda)$. Both Equations (3) and (4) yielded approximately the same result of $\rho_{2.2}(\lambda) = 1.9 \times 10^{-9}$ (km nm)$^{-1}$ for 2.2 km. The $\rho(\lambda)$ value was calculated for $\lambda = 1551.79$ nm but can be calculated for the range of 1530–1565 nm.

2.2.2 | Free-Space Optical segment

For the realisation of the FSO connection, two small-sized air-spaced doublet collimators (Thorlabs, F810APC-1550) with a numerical aperture of 24 mm were employed, dedicated for operation within the C-band. For the alignment of the indoor and outdoor FSO links, a beacon laser at 650 nm was used. The 40-m indoor FSO link was set up in a long corridor, as depicted in Figure 2b, which ensured the protection of the transmission from the outdoor environment. The 100-m outdoor FSO link was established on the rooftop of the PCRL within the NTUA campus. The FSO link is depicted in Figure 2c. Regarding the free-space transmission, a systematic methodology was adopted to effectively model the FSO transmission prior to its establishment. In what follows, we present the modelling approach for our FSO links. The overall channel loss A_{CH}, for the FSO links, was modelled for the wavelength of 1550 nm as follows:

$$A_{ch} = A_A + A_{Geo} + A_C \quad (3)$$

The channel absorption loss A_A(dB) for a link distance z depends on the absorption coefficient $A(\lambda)$ for a specific wavelength λ and can be modelled as [14] follows:

$$A_A = 10 \cdot log_{10}\left(10^{-A(\lambda) \cdot z}\right) \quad (4)$$

In our case, the atmospheric absorption at 1550 nm for the free-space propagation either at 40 or 100 m can be neglected [14]. The geometrical loss A_{Geo} (dB) corresponds to the efficiency due to the geometric characteristics of the receiver (i.e. Rx diameter which equals to 24 mm), whereas A_c refers to the Single Mode Fibre (SMF) coupling loss, namely the fraction of light coupled into the fibre with respect to the incident light on the Rx collimator. A_{Geo} can be calculated by the following equation:

$$A_{Geo} = 10 \cdot log_{10}\left(\frac{D_{Rx}^2}{W(z)^2}\right) \quad (5)$$

where D_{Rx} is the receiver's aperture diameter, and $W(z)$ is the beam size at a distance z from the Tx aperture given by [15]:

$$W(z) = 2 \cdot w_0 + 2 \cdot z \cdot \tan{(\theta/2)} \quad (6)$$

where w_0 is the beam waist at the Tx aperture, $\theta = MFD/f$ is the full-angle beam divergence (in rad) and MFD denotes the Mode-Field-Diameter of an SMF, which typically is equal to 9 μm, whereas f is the focal length of the receiving collimator which equals to 37.13 mm. Since the beam's spot size at 40 m was calculated to be smaller than the receiving aperture diameter (~20 mm), A_{Geo} was set to zero. The coupling loss A_c is the sum of the A_{FC} and A_0. A_{FC} accounts for the effect of turbulence, whereas A_0 accounts for the receiver's coupling characteristics. More specifically, A_{FC} is given by [14] the following equation:

$$A_{FC} = 10 \cdot log_{10}\left[1 + \gamma\left(\frac{D_r}{r_0}\right)^{5/3}\right]^{-\frac{6}{5}} \quad (7)$$

where r_0 is the Fried parameter, and factor γ accounts the level for AO or tip tilt correction in the receiver subsystem (set to 1, 0.28, and 0 for no correction, tip tilt correction and full AO correction.) In both indoor and outdoor FSO links, no

correction was applied; thus, we set γ equal to 1. To account for the optical efficiency and the focal length of the receiving collimator, the optical coupling efficiency A_0 is included as in Ref. [14]:

$$A_0 = 10 \cdot log_{10}\left(2\left(\frac{e^{-\beta^2}}{\beta}\right)^2\right) \quad (8)$$

with

$$\beta = \pi \frac{D_r}{4\lambda}\frac{\omega}{f} \quad (9)$$

where ω is the radius of the MFD [16]. For the case of the 40-m FSO link, since it is located in an indoor environment, the value of Cn^2 has been set to a low value of $10^{-15}m^{-2/3}$, which yields a low Fried parameter value leading to a negligible loss due to turbulence, that is, $A_{FC} \cong 0.02$ dB. The fibre coupling mismatch (due to the geometry of the collimators) is calculated to reach the value of $A_0 \cong 2.1$ dB, which is independent from the link distance. Therefore, the overall 40-m channel link loss is calculated to be almost equal to the optical coupling mismatch loss $A_{ch} \cong 2.13$ dB, as the geometrical loss is calculated to be zero, since the beam spot is smaller than the receiver aperture diameter for link distances shorter than ~50 m. Conversely, for the case of 100-m FSO link, the beam's spot size was calculated to be 41 mm, which is almost double the Rx's aperture resulting in an A_{Geo} of 4.4 dB. To account for varying turbulent losses that depend on the time of day, two different Cn^2 were used: $10^{-14}m^{-2/3}$ for nighttime and $10^{-13}m^{-2/3}$ for daylight. Cn^2 represents the index of refraction structure constant, which measures the atmospheric turbulence affecting the propagation of light in FSO links [14]. Higher Cn^2 values indicate stronger turbulence, leading to potential distortions in quantum signals and impacting the efficiency of the QKD link. During nighttime operation, the A_{FC} was calculated to be negligible (~0.03 dB), whereas during the day, this value increased to 0.26 dB. The experimental results for the 40-m FSO link revealed a minimum overall loss of 4 dB. This value was achieved through manual tip-tilt adjustments and does not include losses from fibre patch cord connectors and the coupling loss of the collimator modules. In contrast, the overall losses for the 100-m FSO link exhibited significant variation, ranging from 10 to 18 dB depending on the time of operation. Notably, during the experiment days, increased wind speeds led to the pointing instability of the two collimators, primarily due to the absence of an active stabilisation mechanism. An additional loss of about 2 dB was attributed to the patch cords and the multiple connection (eight) points extending from the rooftop to the laboratory. Figure 4 provides the theoretical calculated and experimental values of different FSO link losses varying from 40 to 100 m. The overall link loss is mainly attributed to the optical coupling loss, which remains constant over distance, and the geometrical loss, which increases quadratically over distance. In Figure 4, a loss

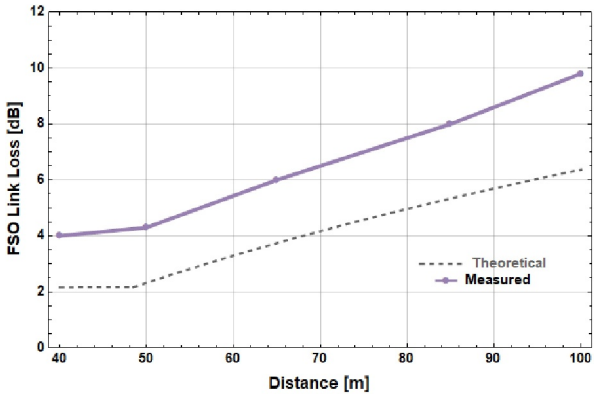

FIGURE 4 FSO Link Loss versus Distance (m). FSO, Free-Space Optical.

difference of about 2 dB is evident between the theoretical and the experimental values. This difference may be attributed to the manual steering of the collimators, resulting in loss due to the off-axis, angular and axial deviation [17], which were not included in the theoretical calculations provided above.

2.2.3 | Methodology for the quantum layer

To evaluate the performance of all the transmission scenarios described above, the following methodology was adopted. Given that Alice's vertically polarised photons were aligned with the vertical transmission port of the PBS through the PC, the prepared single photons should only be detected by SPAD 1. Consequently, one can derive from the count rate of SPAD 2, the clicks that originate from the imperfect PBS visibility after extracting the SPADs Dark Count Rates (DCR). To continue, if noise is added to the transmission link, an increase in both SPADs will be observed. By specifically identifying and measuring the amount of false clicks via photon counting measurements, the QBER in Z-basis can be expressed as the ratio of false detector clicks to the total clicks in both detectors, represented by the following equation:

$$QBER = \frac{1}{2}\frac{N_{ap} + N_{DCR1} + N_{DCR2} + N_{Noise} + 2N_{PBS}}{N_{total}} \quad (10)$$

where N_{signal} stands for the counts recorded in SPAD1. N_{DCR1} and N_{DCR2} denote the DCR of each detector, which were measured as 15 and 18 counts per second (cps), respectively, N_{Noise} represents background noise photons stemming from the transmission of the classical signal in both detectors, N_{PBS} accounts for the imperfect visibility of the PBS1 in the emission station during the preparation of vertically polarised photons as well as for the counts detected at SPAD2 due to the imperfect visibility of the PBS2 in the receiver (approximately 99%). N_{ap} signifies the afterpulsing contribution counts, which, when divided by N_{total}, yields the afterpulsing probability, which was measured to be about 2% under the above

mentioned SPAD driving characteristics [12]. The factor 1/2 is introduced in Equation (10) because each noise photon has a 50% likelihood of being recorded as an erroneous count, whereas erroneous clicks originating from the imperfect PBS visibility do not. Employing the presented experimental setup, the values used above can be quantified, allowing to calculate the expected QBER in the Z-basis. It is worth noting that this equation does not encompass errors arising from the imperfect visibility of a QKD polarisation encoder since only a single polarisation state is transmitted. Recently, published works in the literature have focused on estimating the intrinsic-QBER (i-QBER) arising from imperfections in polarisation-based QKD sources. Extremely low i-QBER values below 0.5% have been reported [18, 19]; therefore, this contribution was not included in our theoretical calculations.

2.2.4 | Semi-empirical software tool for Secure Key Rate calculation

Apart from the QBER measurements, that are directly derived from the SPADs click rates, a semi-empirical software tool was developed to calculate the expected SKR for the weak-vacuum Decoy State BB84 protocol, as described by Ma [20]. According to [20], the SKR value is bounded by the following equation:

$$SKR \geq f_{rep} q \left\{ Q_1 [1 - H_2(e_1)] - Q_\mu f(E_\mu) H_2(\mathrm{E}_\mu) \right\} \eta_{dead} \quad (11)$$

In this equation, f_{rep} represents the transmitter's emission rate, q signifies the protocol efficiency, μ represents the average photon number per signal in signal states, Q_μ and E_μ are the gain and QBER of signal states, Q_1 and e_1 denote the gain and error rate of the single photon state in signal states, respectively, $f(x)$ is the bi-directional error correction rate, $H_2(x)$ is the binary entropy function, and η_{dead} represents the detectors' deadtime efficiency. The gain of the signal state is determined by the following expression [21]:

$$Q_\mu = Y_0 + 1 - \exp(-\eta\,\mu) \quad (12)$$

where η corresponds to the overall link transmittance, and Y_0 corresponds to the chance probability of detector firing due to noise, which includes dark counts, Raman noise counts, cross-talk noise, background and solar noise or afterpulsing effects, expressed as follows:

$$Y_0 = P_{dcr} + P_{ram} + P_{x-talk} + P_{back} + P_{ap} \quad (13)$$

For this study, the measured values of the overall noise (Y_0) and the link's transmittance (η) along with the system assumptions (f_{rep}, dead time (τ_d), Q.E) have been fed to the Equation 12, to calculate the expected signal gain. In turn, one can calculate the values of Q_1 and E_μ according to [20]. The values calculated via the software are in good agreement with the values derived from the experimental measurements according to Eq. 10, as was also presented in Refs. [12, 22]. Finally, by including the probability of transmitting a signal, decoy or vacuum state, the SKR can be obtained by Equation 11. According to [20], for this study, it is assumed that the protocol selects to transmit signal, decoy, and vacuum states with probabilities of 66.4%, 29.3%, and 4.2%, respectively (resulting in a protocol efficiency of approximately $q = 1/3$). Additionally, the bi-directional error correction efficiency $f(e)$ was set to 1.22, corresponding to the CASCADE error correction algorithm [5]. Finally, since the signal and decoy gain values are calculated by the links transmittance (η) and system assumptions ($f_{rep}, \tau_d, Q.E$) values, the dead time correction should be included. The dead time correction efficiency (η_{dead}) is included in Equation 11 as described in Ref. [5].

3 | RESULTS AND DISCUSSION

3.1 | Fibre segment

The aforementioned methodology has been applied to the scenarios discussed in Section 2. To evaluate their performance, at first, regarding the 2.2-km fibre segment, before multiplexing the quantum signal with the classical ones, the performance in the dark fibre scenario was evaluated, revealing a QBER value of 1.23% which yielded an expected SKR of 1.7 kbps. Subsequently, the best-case and worst-case classical wavelength allocations have been identified. More specifically, at first, we chose to coexist the quantum signal with CW classical signals in the vicinity of quantum signal (1.5–2 nm apart), that is, λ_1 = 1551.8 nm, λ_2 = 1549.5 nm, λ_3 = 1552.0 nm, and λ_4 = 1549.0 nm. Each of the classical signals was launched with a power level of 0 dBm into the IC fibre resulting in a total launched optical power of +6 dBm. As can be seen from Figure 5a, Quantum Bit Error Rate values (<8%) were obtained even when all four classical signals co-propagated with the quantum signal. However, when the classical signals were spectrally allocated 9–10 nm apart from the quantum signal, specifically at λ_1 = 1562 nm, λ_2 = 1560 nm, λ_3 = 1532 nm, and λ_4 = 1530 nm, QBER values exceeded 8% even with just λ_1 and λ_2 present alongside the quantum signal. By employing the developed software toolbox employing the weak decoy and vacuum state BB84 protocol, SKR values for the best and worst-case WDM allocation scenario were calculated. Indicatively, for the best-case WDM allocation scenario, the expected SKR varied from 1011 bps (coexistence with λ_1) down to just 5 bps when all four wavelengths coexisted in the same fibre. On the contrary, for the worst-case WDM allocation, SKR values could not be extracted when more than two wavelengths coexisted. More specifically, a SKR of 500 bps was found for λ_1 = 1562 nm and λ_2 = 1560 nm. To further evaluate the performance of the fibre transmission, stability measurements were conducted for the best-case WDM allocation scenario. The 2.2-km IC fibre transmission exhibited robust performance in terms of stability for over an hour, consistently showcasing acceptable QBER

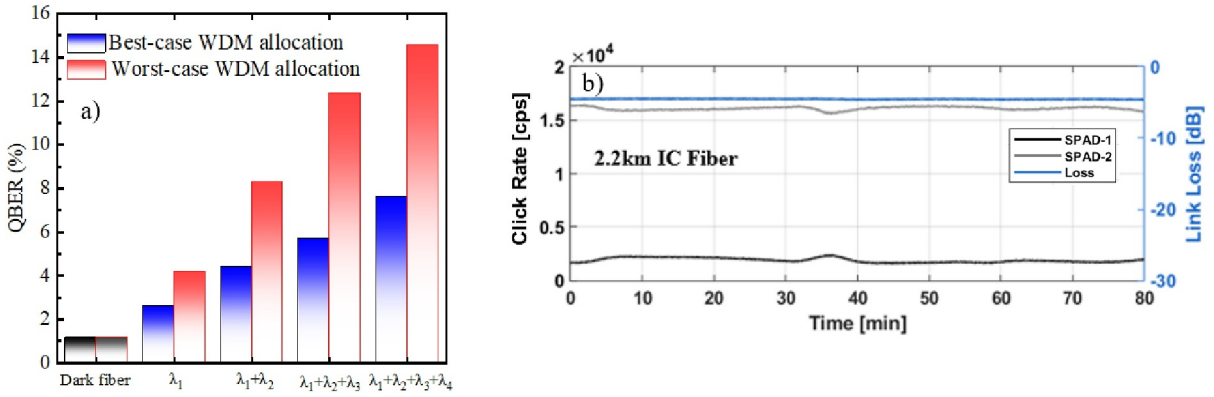

FIGURE 5 (a) QBER versus wavelengths for worst (red) and best (blue) WDM allocation scenarios. (b) Link loss and measured detection click rate over time for the 2.2-km IC fibre. IC, Intra-Campus; QBER, Quantum Bit Error Rate; WDM, Wavelength-Division Multiplexing.

values below 7.0%. As depicted in Figure 5b, small instabilities between the 30- and 40-min mark (indicated by a small increase and decrease in counts of SPAD1 and SPAD 2, respectively) are evident. Notably, these instabilities are due to the cumulative action of polarisation drifts and laser shot noise. More specifically, within this hour, the polarisation drifts were estimated to be in the order of ±400 cps, whereas the shot noise contribution was ca. 120 cps. These polarisation drifts seem to be generally slow; therefore, they could be easily compensated with an active polarisation control element.

3.2 | Free-Space Optical segment

For the evaluation of the free-space segment, both a 40-m indoor and a 100-m outdoor link have been established. Figure 6 presents the link loss over time for the 40-m indoor FSO link, estimated via the clicks per second measurement of both detectors, as well as the clicks registered by each detector. Since the link was set up in an indoor environment, it was protected from most of the environmental disturbances, such as noise or wind. Both the link and the polarisation stability have proven to be stable. Small drifts in polarisation may be attributed to the several metres of fibre transmission (~60 m of patch cords). The measured loss of the 40-m link was found to be 5 dB, aligned with our theoretical calculations. Quantum Bit Error Rate values of 1.36% over a period of 1 h, which in turn yielded an expected SKR value of 490 bps according to (11). Furthermore, the free-space quantum link exhibited minimal interference when co-propagating with classical signals, managing to maintain acceptable QBER values even at launch power intensities as high as +5 dBm with a calculated SKR of 880 bps. On the contrary, the 100-m rooftop FSO link has proven to be much less stable over time since it was installed in an outdoor environment, making it susceptible to misalignment caused by wind.

In Figure 7 below, the performance of the 100-m outdoor FSO link is presented under over both daylight and nighttime operation. In both cases, the quantum signals coexisted with a single CW wavelength centred at 1551.8 nm with 0 dBm

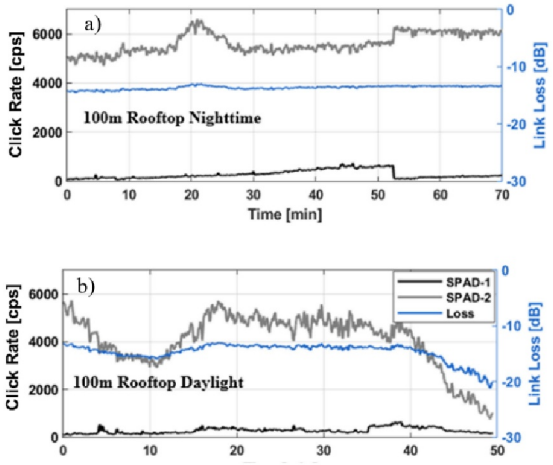

FIGURE 6 Link loss and detection rates over time for a 100-m FSO link under (a) nighttime and (b) daylight. FSO, Free-Space Optical.

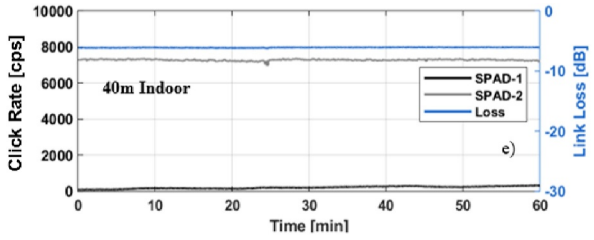

FIGURE 7 Link loss and detection counts over time for the 40-m FSO link. FSO, Free-Space Optical.

launch power. During nighttime operation (Figure 7a), the overall link loss remained stable at around 12 dB (including a fibre patch cord length of about 200 m) in agreement with our theoretical toolbox in Section 2. Since in the indoor scenario the polarisation drifts were negligible, the polarisation drifts in the outdoor scenario are mainly attributed to displacement of the fibre patch cords due to the windy conditions during the night. Finally, regarding the daylight operation scenario, the overall link loss strongly varied from 12 dB up to 20 dB

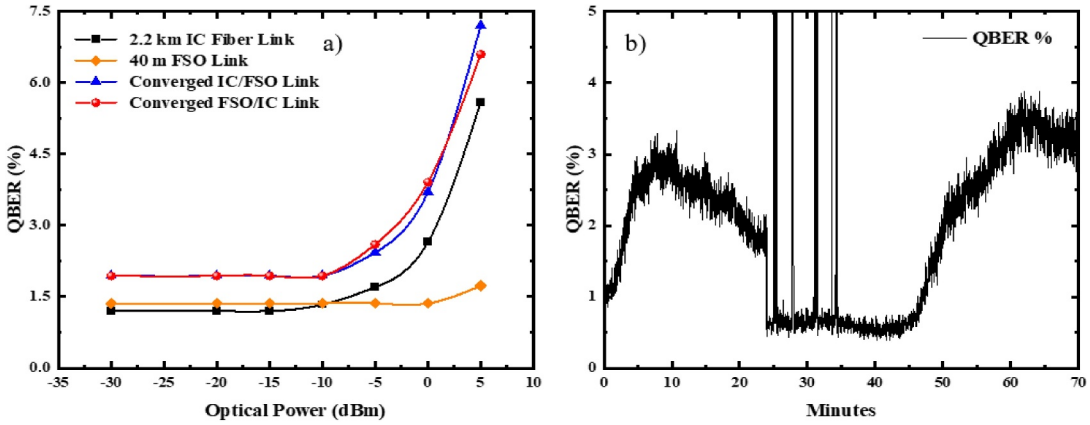

FIGURE 8 (a) QBER (%) versus. Optical Power, (b) QBER measurement over time for the converged Fibre/FSO link. FSO, Free-Space Optical; QBER, Quantum Bit Error Rate.

(Figure 7b). This instability resulted in a reduction of the total number of clicks over time in both detectors and finally resulted in the total loss of the link after about 50 min. This behaviour is explained by the increased wind speeds that were present during the daytime, resulting in instability in the pointing of the two collimators, since no active stabilisation mechanism was used. It is worth noting that despite ample sunlight during the day of the experimental campaign, there was no significant increase in background noise. The fibre coupling, which also acts as a spatial filter, along with the narrow band pass spectral as well as temporal filters that were used, managed to eliminate the solar radiance photons (from 15 kcps (free running mode) down to 70 cps (gated mode)). Quantum Bit Error Rate values lower than 3.2% were observed within the first 40 min of operation yielding an expected SKR of about 600 bps for both nighttime and daytime operation, since the minimum loss of the link was the same (~12 dB) for both operation scenarios, revealing that a QKD FSO could also be operational during the day.

3.3 | Converged fibre/Free-Space Optical segment

For the evaluation of the converged fibre/free-space segment, the 40-m indoor link has been integrated with the 2.2-km IC fibre link. The optical loss introduced by the installed fibre link was measured to be 4.5 dB (including the loss stemming from the multiple connection points) at 1550 nm. For the FSO link, a coupling efficiency of 32% was achieved, which corresponds to 5 dB optical loss mainly due to SMF coupling efficiency aligning with our theoretical calculations. The shorter indoor FSO link was selected for the converged scenario due to its superior stability over time and simpler installation configuration. Figure 8a displays the determined QBER values across different launched optical power levels of the classical wavelength (λ_1 = 1551.8 nm) in three distinct transmission scenarios for comparison purposes. Notably, for the converged fibre/FSO link, QBER values remained below 3.5% at a launch power of 0 dBm, whereas in the 40-m FSO link scenario, the QBER values were even more favourable, staying below 1.7% for optical power levels up to +5 dBm. This enhanced performance in the FSO link can be ascribed to the absence of SpRS noise photons, a challenge encountered in the IC fibre link scenario. Conversely, when using the IC fibre link as the propagation medium, there was a marked escalation in QBER values, which began to rise exponentially as the launched power levels exceeded −10 dBm. It is also worth noting that no difference in the performance is observed when the free-space transmission is prior to the fibre one or vice versa as can be seen in Figure 8a. This was the expected outcome, since the main noise contributor for the converged scenario is Raman noise counts, which increase linearly with the classical signal launch power [5]. Lastly, Figure 8b showcases a stability measurement, in the absence of classical signal transmission, spanning 70 min for the converged fibre/FSO scenario. Remarkably, the fibre/FSO configuration displayed several minutes stability without any applied correction, maintaining a QBER consistently below 5%. The fluctuations in QBER can primarily be attributed to polarisation drifts originating from the fibre-based components and the IC transmission, since the indoor 40-m FSO has been proven to be generally stable. The sharp increases observed in Figure 8b are indicative of interruptions or blockages in the FSO link. Figure 9 summarises all the expected SKRs as calculated from the software toolbox versus the launched optical power of the classical signal for all scenarios discussed above.

As it is evident, the FSO transmission is more robust to noise than the fibre one due to the SpRS noise as discussed in detail above.

4 | CONCLUSIONS

In summary, this work focused on experimentally evaluating the QKD integration across various transmission scenarios, employing cost-effective components and a simplified setup. This setup enabled us to benchmark segments where classical

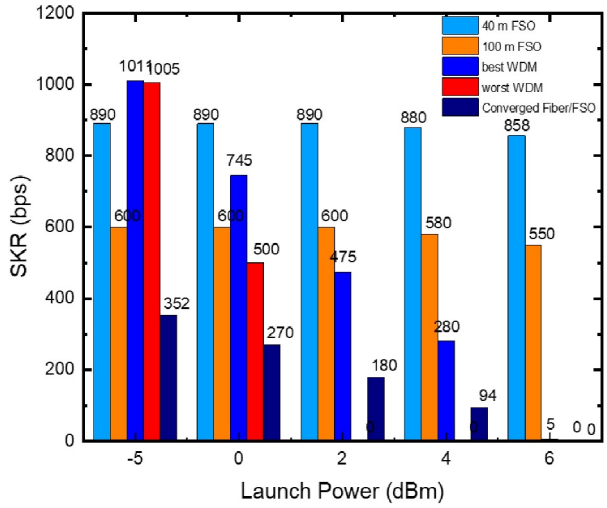

FIGURE 9 SKR values versus Launch Power (dBm) for all the scenarios. SKR, Secure Key Rate.

and quantum signals coexist. Specifically, we evaluated both fibre and FSO scenarios, demonstrating the potential for integrating these segments by also exploring converged scenarios. For the fibre segment, we characterised a 2.2-km installed fibre in terms of losses and its Raman noise profile, while for the FSO segment, we utilised a comprehensive theoretical approach to evaluate and characterise loss. Our presented work can be found useful for the early-stage of deployment tests targeting several use-case demonstrations of QKD systems in deployed fibre and FSO networks. Through our reference setup for QBER measurements and the integration of a semi-empirical software tool, we calculated the expected SKRs employing the weak decoy vacuum BB84 protocol. Our results offer valuable insights into the practical implementation of QKD in everyday scenarios, particularly within metropolitan fibre/FSO links carrying classical traffic. This approach not only underscores the versatility and potential of QKD in a variety of settings but also enhances its accessibility, paving the way for a broader adoption of quantum secure communication technologies.

AUTHOR CONTRIBUTIONS

Aristeidis Stathis: Conceptualisation; Investigation; Methodology; Software; Visualisation; writing–original draft; Writing–review & editing. **Argiris Ntanos:** Conceptualisation; Investigation; Methodology; Software; Visualisation; Writing–original draft; Writing–review & editing. **Panagiotis Toumasis:** Investigation; Methodology. **Nikolaos K. Lyras:** Conceptualisation; Investigation; Methodology; Writing–original draft; Writing–review & editing. **Giannis Giannoulis:** Conceptualisation; Investigation; Methodology; Visualisation; Supervision; Writing–original draft; Writing–review & editing **Hercules Avramopoulos:** Funding acquisition; Project administration; Resources.

ACKNOWLEDGEMENTS

This work has received funding from the European Union's Horizon Europe Research and Innovation programme under the project "Quantum Security Networks Partnership" (QSNP, Grant Agreement No 101114043). This work has been supported by the project HellasQCI, under grant agreement No.101091504. Views and opinions expressed are, however, those of the authors only and do not necessarily reflect those of the European Union. The European Union cannot be held responsible for them.

CONFLICT OF INTEREST STATEMENT

The author declares no conflict of interest.

DATA AVAILABILITY STATEMENT

The data that support the findings of this study are available from the corresponding author upon reasonable request.

ORCID

Aristeidis Stathis https://orcid.org/0000-0002-1598-7122
Argiris Ntanos https://orcid.org/0000-0002-0142-5831
Panagiotis Toumasis https://orcid.org/0000-0002-6378-8232
Nikolaos K. Lyras https://orcid.org/0000-0002-6964-8185
Giannis Giannoulis https://orcid.org/0000-0002-5825-5597
Hercules Avramopoulos https://orcid.org/0000-0001-8793-2262

REFERENCES

1. Bennett, C.H., et al.: Experimental quantum cryptography. J. Cryptol. 5(1), 3–28 (1992). https://doi.org/10.1007/BF00191318
2. Hughes, R.J., et al.: Practical free-space quantum key distribution over 10 km in daylight and at night. New J. Phys. 4(1), 43 (2002). https://doi.org/10.1088/1367-2630/4/1/343
3. Peng, C.-Z., et al.: Experimental free-space distribution of entangled photon pairs over 13 km: towards Satellite-based global quantum communication. Phys. Rev. Lett. 94(15), 150501 (2005). https://doi.org/10.1103/PhysRevLett.94.150501
4. Schmitt-Manderbach, T., et al.: Experimental demonstration of free-space decoy-state quantum key distribution over 144 km. Phys. Rev. Lett. 98(1), 010504 (2007). https://doi.org/10.1103/PhysRevLett.98.010504
5. Eraerds, P., et al.: Quantum key distribution and 1 Gbps data encryption over a single fibre. New J. Phys. 12(6), 063027 (2010). https://doi.org/10.1088/1367-2630/12/6/063027
6. Majumdar, A.K.: Advanced free space optics (FSO): a systems approach. In: Springer Series in Optical Sciences, vol. 186. Springer New York, New York (2015). https://doi.org/10.1007/978-1-4939-0918-6
7. Avesani, M., et al.: Full daylight quantum-key-distribution at 1550 nm enabled by integrated silicon photonics. Npj Quan. Inf. 7(1), 93 (2021). Art. no. 1. https://doi.org/10.1038/s41534-021-00421-2
8. Gong, Y.-H., et al.: Free-space quantum key distribution in urban daylight with the SPGD algorithm control of a deformable mirror. Opt. Express 26(15), 18897–18905 (2018). https://doi.org/10.1364/OE.26.018897
9. Vedovato, F., et al.: Realization of intermodal fiber/free-space quantum key distribution networks. In: Hemmer, P.R., Migdall, A.L. (eds.) Quantum Computing, Communication, and Simulation III, pp. 96. SPIE, San Francisco (2023). https://doi.org/10.1117/12.2668341

10. Picciariello, F., et al.: Intermodal quantum key distribution field trial with active switching between fiber and free-space channels. arXiv, Oct. 26 [Online]. http://arxiv.org/abs/2310.17441 (2023). Accessed: 30 Jan 2024
11. Bulla, L., et al.: Distribution of genuine high-dimensional entanglement over 10.2 km of noisy metropolitan atmosphere. Phys. Rev. A. 107(5), L050402 (2023). https://doi.org/10.1103/PhysRevA.107.L050402
12. Ntanos, A., et al.: Deployment-oriented classical/quantum coexistence in X-Haul fiber link for B5G networks. In: Conference on Lasers and Electro-Optics (2023), Paper AM3N.5. Optica Publishing Group (2023). AW3N.5.
13. Stathis, A., et al.: Coexistence of Quantum/Classical Signals Over Converged Fiber/FSO Links for Intra-Campus Networking
14. Andrews, L.C., Phillips, R.L.: Laser Beam Propagation through Random Media, 2nd ed SPIE Press, Bellingham (2005)
15. Schulz, D., et al.: Robust optical wireless link for the backhaul and fronthaul of small radio cells. J. Light. Technol. 34(6), 1523–1532 (2016). https://doi.org/10.1109/JLT.2016.2523801
16. Ruilier, C., Cassaing, F.: Coupling of large telescopes and single-mode waveguides: application to stellar interferometry. J. Opt. Soc. Am. A Opt. Image Sci. Vis. 18(1), 143–149 (2001). https://doi.org/10.1364/JOSAA.18.000143
17. Zhang, X., et al.: Characteristics of collimators based on the large-mode-area CMCF for coupling laser beam. Appl. Sci. 11(24), 11604 (2021). https://doi.org/10.3390/app112411604
18. Agnesi, C., et al.: All-fiber self-compensating polarization encoder for quantum key distribution. Opt. Lett. 44(10), 2398–2401 (2019). https://doi.org/10.1364/OL.44.002398
19. "Robust polarization state generation for long-range quantum key distribution." Accessed: Jul. 26, 2023. [Online]. https://opg.optica.org/oe/fulltext.cfm?uri=oe-31-9-13700&id=529021
20. Ma, X., et al.: Practical decoy state for quantum key distribution. Phys. Rev. A. 72(1), 012326 (2005). https://doi.org/10.1103/PhysRevA.72.012326
21. Lo, H.-K., Ma, X., Chen, K.: Decoy state quantum key distribution. Phys. Rev. Lett. 94(23), 230504 (2005). https://doi.org/10.1103/PhysRevLett.94.230504
22. Stathis, A., et al.: Coexistence of quantum/classical signals over converged fiber/FSO links for intra-campus networking. In: P69. Glasgow (2023)

How to cite this article: Stathis, A., et al.: Experimental feasibility analysis of quantum/classical coexistence over fibre and free space links. IET Quant. Comm. 5(4), 575–585 (2024). https://doi.org/10.1049/qtc2.12097